SIAM J. Applied Dynamical Systems
Vol. 19, No. 4, pp. 2829–2846

Sequential Escapes and Synchrony Breaking for Networks of Bistable Oscillatory Nodes*

Jennifer Creaser†, Peter Ashwin†, and Krasimira Tsaneva-Atanasova‡

Abstract. Progression through different synchronized and desynchronized regimes in brain networks has been reported to reflect physiological and behavioral states, such as working memory and attention. Moreover, intracranial recordings of epileptic seizures show a progression towards synchronization as brain regions are recruited and the seizures evolve. In this paper, we build on our previous work on noise-induced transitions on networks to explore the interplay between transitions and synchronization. We consider a bistable dynamical system that is initially at a stable equilibrium (quiescent) that coexists with an oscillatory state (active). The addition of noise will typically lead to *escape* from the quiescent to the active state. If a number of such systems are coupled, these escapes can spread sequentially in the manner of a "domino effect." We illustrate our findings numerically in an example system with three coupled nodes. We first show that a symmetrically coupled network with amplitude-dependent coupling exhibits new phenomena of *accelerating* and *decelerating* domino effects modulated by the strength and sign of the coupling. This is quantified by numerically computing escape times for the system with weak coupling. We then apply phase-amplitude-dependent coupling and explore the interplay between synchronized and desynchronized dynamics in the system. We consider *escape phases* between nodes where the cascade of noise-induced escapes is associated with various types of partial synchrony along the sequence. We show examples for the three-node system in which there is multistability between in-phase and antiphase solutions where solutions switch between the two as the sequence of escapes progresses.

Key words. generalized Hopf normal form, escape phase, escape time, sequential escape, noise-induced transition

AMS subject classifications. 92C42, 34D06, 37H20, 37G05

DOI. 10.1137/20M1345773

1. Introduction.

A widely observed pattern of activity in the mammalian cortex comprises the sequential switching between periods of quiescence (i.e., Down states) and periods of firing activity (i.e., Up states) [27, 36]. Such Up-Down states in cortical dynamics are

*Received by the editors June 16, 2020; accepted for publication (in revised form) by J. Rubin October 7, 2020; published electronically December 17, 2020.
https://doi.org/10.1137/20M1345773
Funding: This research was supported by EPSRC Centre for Predictive Modeling in Healthcare grant EP/N014391/1, and by the Technical University of Munich – Institute for Advanced Study funded by the German Excellence Initiative. The work of the first author was also supported by MRC Skills Development Fellowship MR/S019499/1.
†Department of Mathematics, University of Exeter, Exeter, EX4 4QF, UK, and EPSRC Centre for Predictive Modelling in Healthcare, University of Exeter, Exeter, EX4 4QJ, UK (j.creaser@exeter.ac.uk, p.ashwin@exeter.ac.uk).
‡Department of Mathematics and Living Systems Institute, University of Exeter, Exeter, EX4 4QF, UK; EPSRC Centre for Predictive Modelling in Healthcare, University of Exeter, Exeter, EX4 4QJ, UK; Institute for Advanced Study, Technical University of Munich, D-85748 Garching, Germany; and Department of Bioinformatics and Mathematical Modelling, Institute of Biophysics and Biomedical Engineering, Bulgarian Academy of Sciences, 1113 Sofia, Bulgaria (K.Tsaneva-Atanasova@exeter.ac.uk).

thought to reflect transitions between attractors in networks of bistable nodes [21, 23]. Moreover, these cortical dynamics involve transitions through different synchronized and desynchronized regimes that reflect physiological and behavioral states, including working memory and attention [19]. A recent study demonstrates transitions between a 'synchronized' state during sleep and a "desynchronized" state during wakefulness in the population activity in prefrontal cortical networks of freely moving macaques [30]. Furthermore, dynamic evolution of synchronization has been associated with epileptiform phenomena and, in particular, seizures [24]. Indeed, a study of ECoG (electrocorticography) recordings consisting of focal-onset seizures [28] reports that in the majority of cases, there is a progression towards synchronization as the seizures evolve. Characterizing possible scenarios for such dynamic synchronization can contribute to better understanding of cortical dynamics and improved epilepsy diagnosis and treatment.

Recently, phase-amplitude coupling has been attracting increased attention due to its potential for understanding the generation of brain activity in health and pathology [35]. Phase-amplitude coupling has been implicated as a general mechanism for memory consolidation [11], in pathological synchronization during sleep in Parkinson's disease [20], and, in general, of importance in modeling brain dynamics [17], including the spatiotemporal dynamics preceding neocortical seizures [12]. Furthermore, phase-amplitude coupling has physiological application to hormone dynamics, for example, coupling between ultradian and circadian rhythms in stress hormones, such as cortisol [38], as well as the well-known amplitude (and frequency) modulation of luteinizing hormone rhythms during the menstrual cycle [13, 18, 33].

In this paper we focus on transient noise-induced behavior in networks of asymmetric bistable attractor systems. We consider noise-induced escapes in a system consisting of Hopf normal forms coupled with amplitude only and phase-amplitude coupling. Models of two complex coupled Bautin-type elliptic bursters have been shown to exhibit within-burst changes of synchrony in the absence of noise [4]. This phenomenon is preserved with biologically motivated (synaptic or gap-junction) coupling functions [34]. Bistability of in-phase and antiphase solutions of two coupled Wilson–Cowan oscillators near a Hopf bifurcation was recently shown to have applications to perceptual bistability [32]. Additionally, there have been various studies of noise-induced transitions in networks of symmetric [7, 8, 31] and asymmetric [29, 2, 3] bistable attractors. However, to the best of our knowledge, synchrony changes during sequential escape have not been previously investigated.

We consider networks of nodes $z_k \in \mathbb{C}$ given by the system of Itô stochastic differential equations (SDEs),

$$\mathrm{d}z_k(t) = \left[f(z_k) + \sum_{j \neq k} A_{jk}\, g(z_j, z_k) \right] \mathrm{d}t + \alpha\, \mathrm{d}W_k(t), \tag{1.1}$$

where intrinsic node dynamics are given by f, and interaction between nodes is governed by the coupling function g and adjacency matrix $A_{ij} \in \mathbb{R}$. Each node has an additive independent identically distributed (i.i.d.) complex valued Wiener process W_k with amplitude $\alpha > 0$.

We choose f such that each uncoupled node is asymmetrically bistable, where there is a weakly stable equilibria attractor and a more strongly attracting oscillatory attractor. We consider noise-induced switching between the two states; starting in the weakly stable state we

say a node *escapes* when it crosses the threshold to the basin boundary of the other state. In the presence of low noise each node transitions from the weakly stable state to the oscillatory state. The asymmetry of the system means that transitions back to the weakly stable state occur on a much longer timescale and can be ignored. This gives a domino-like cascade of sequential escapes across the network. In our previous work we show that domino-like cascades are modulated by the strength and the form of coupling [2, 3, 14].

Previously, we considered a simple bistable model where the stable states of f are equilibria given by an asymmetric case of the Schlögl model [29] with linear diffusive coupling g [2]. We introduce the *fast-domino* and *slow-domino* regimes of sequential escapes. These regimes are delineated by bifurcations on the basin boundaries of the attractors. In particular, for two strongly coupled nodes, escape of both nodes is almost simultaneous giving a fast-domino effect. For weakly coupled nodes we show that although the escapes are predetermined by the noise, the coupling permutes the potential landscape in a way that induces a delay between sequential escapes, giving a slow-domino effect. Introducing nondiffusive coupling of Gaussian form, so-called *pulse* coupling, we show that the slow-domino effect can also be achieved via a a global saddle connection bifurcation in which the most likely escape path from one attractor hits the escape saddle from the basin boundary of another partially escaped attractor [3]. For networks with both diffusive and nondiffusive couplings we show that in an asymmetrically coupled network of three nodes the slow-domino regime affects not only the speed of escape but also the order, making some sequences of escape much more likely than others.

We extend the work of [2] in [14] in which we use a truncated form of a Bautin bifurcation for f where the strongly attracting stable state is a periodic orbit. Here, the conversion to polar coordinates provides information on the behavior of both the phase and the amplitude. In this case, the phase and amplitude decouple, and we consider only the behavior of the amplitude system, fixing the frequency of the oscillatory dynamics of the nodes throughout. We use first passage time theory to compute a closed form of the mean escape time for one uncoupled node. In a two-node system with either bidirectional, unidirectional, or uncoupled nodes we identify critical values of the coupling at which the qualitative behavior of the sequential escapes changes. We explain the scalings of mean escape times for each network as a function of coupling strength using multidimensional Eyring–Kramers escape time theory [9, 16, 26]. In particular, for strong bidirectional coupling we show that the time of the first node to escape is greatly increased, but the following escape times are greatly reduced, giving the fast-domino effect.

In this paper, we investigate the interplay of phase and escape in networks of bistable nodes where the individual node dynamics are given by

$$f(z) = (-\nu + i\omega)z + (2 + i\eta)z|z|^2 - (1 + i\delta)z|z|^4. \tag{1.2}$$

This is a general form of the Bautin model studied in [5, 14] where (1.2) has additional phase parameters η and δ. The one-node system can undergo a coordinate change (near identity transform) that effectively removes complicated phase dynamics from the behavior of the system. The system then behaves as in [14]. In the coupled system (1.1) the phase dynamics cannot be removed by a coordinate change and will play a crucial role in the behavior of the system. In [14] all escapes occur at $\theta = 0$ in the two-node case, as phase was constant for all R.

Here, the phase depends on R, and there will be a genuine interplay between synchrony and escape. This idealized system was chosen to allow some analysis on the synchronous states.

The layout of the paper is as follows. We present a brief overview of one-node dynamics in section 2 and then focus on all-to-all coupled systems of at least three nodes. In line with our previous work, we begin our network analysis by considering amplitude-only coupling in section 3. We show that the strength and sign of the coupling lead to a new phenomenon of *accelerating* or *decelerating* domino effect, and we numerically compute the escape times for the system with weak coupling. In section 4 we consider phase-amplitude coupling and explore the interplay between synchronized and desynchronized dynamics in the system. We analyze the amplitude and phase dynamics in a neighborhood of the limit cycles of escape states of the system. We show examples for the three-node system in which there is multistability between in-phase and antiphase solutions, and we show that solutions switch between the two with subsequent escapes.

2. Noise-induced transitions of a single node. We start by considering system (1.1) with (1.2) for $k = 1$ uncoupled node,

$$\mathrm{d}z(t) = \left[(-\nu + i\omega)z + (2 + i\eta)z|z|^2 - (1 + i\delta)z|z|^4\right]\mathrm{d}t + \alpha\,\mathrm{d}W(t), \tag{2.1}$$

where $W \in \mathbb{C}$ and $\nu, \omega, \eta, \delta \in \mathbb{R}$. As in [14] we restrict $0 < \nu < 1$ such that the noise-free system $\alpha = 0$ has a stable equilibrium and a stable periodic orbit separated by an unstable periodic orbit. The periodic solutions are eliminated in a saddle node bifurcation at $\nu = 1$, and for $\nu > 1$ only the stable equilibrium prevails. At $\nu = 0$ there is a subcritical Hopf bifurcation, and for $\nu < 0$ there are one stable periodic orbit and an unstable equilibrium. We fix $\nu = 0.1$ throughout this paper, which means that the rate of noise-induced escape from the stable equilibrium is much higher than from the stable periodic. We are interested in understanding properties of coupled systems of the form (2.1) for weak noise, i.e., small α. In practice, we fix on $\alpha = 0.035$ as a compromise between (1) mean escape times that are long enough to observe details of successive escapes, and (2) manageable computation time of the simulations; this trade-off is discussed in section 5. Figure 1(a)–(b) shows one realization of the single node dynamics for

$$\nu = 0.1,\ \omega = 0.3,\ \eta = 1.0,\ \delta = 0.4,\ \alpha = 0.035. \tag{2.2}$$

The dynamics' realizations are computed using the stochastic Heun method in MATLAB (version 2018b) with the initial condition $z = 1 + 0i$ and step size $h = 10^{-2}$.

We transform (2.1) into polar coordinates given by $z(t) = R(t)\exp[i\theta(t)]$ with $R(t) \geq 0$ and $\theta(t)$ considered modulo 2π. This gives

$$\mathrm{d}R = \left[F(R) + \frac{\alpha^2}{2R}\right]\mathrm{d}t + \alpha \mathrm{d}W_R, \tag{2.3a}$$

$$\mathrm{d}\theta = \Omega(R)\mathrm{d}t + \frac{\alpha}{R}\mathrm{d}W_\theta, \tag{2.3b}$$

where we define

$$F(R) := [-\nu + 2R^2 - R^4]R, \tag{2.4a}$$

$$\Omega(R) := \omega + \eta R^2 - \delta R^4. \tag{2.4b}$$

Note that (2.3a) is independent of θ as in [14]. Considering (2.3a) as a potential problem for $R(t)$,

$$\mathrm{d}R = -\frac{\partial V}{\partial R}\mathrm{d}t + \alpha \mathrm{d}W_R,$$

gives the potential function

$$V := \frac{\nu R^2}{2} - \frac{R^4}{2} + \frac{R^6}{6} - \frac{\alpha^2}{2}\ln R. \tag{2.5}$$

The equilibrium and periodic orbits form two minima and one maximum.

For $\alpha = 0$ we find an equilibrium at $R_{\min} = 0$ and for $0 < \nu < 1$ find periodic orbits at

$$R_c = \sqrt{1 - \sqrt{1-\nu}}, \quad R_{\max} = \sqrt{1 + \sqrt{1-\nu}},$$

where R_c is linearly unstable, and $R_{\max}$ is linearly stable. Figure 1(c) shows (2.4a) with $R_{\min}$, R_c, and $R_{\max}$ for parameters (2.2). In the noise-free case, the potential barrier or *gate* between the basins of the two attractors is given by R_c. For $\alpha > 0$ the potential barrier decreases until $R_{\min}$ and R_c undergo a saddle node bifurcation, and for $\alpha > \nu/2$ only $R_{\max}$ exists, and the dynamics are dominated by noise. A full treatment of the interplay between the ν and α can be found in [14].

Unlike in [14], (2.4b) depends on R due to the addition of generic phase terms, and the system does not decouple. Figure 1(d) shows (2.4b) against R for parameters (2.2). In particular, the periodic orbits have angular frequencies

$$\Omega_c = \omega + \eta R_c^2 - \delta R_c^4 \quad \text{and} \quad \Omega_{\mathrm{s}} = \omega + \eta \mathrm{R}_{\mathrm{s}}^2 - \delta \mathrm{R}_{\mathrm{s}}^4$$

that, in general, are different from each other and from the Hopf frequency ω. Note that

$$\frac{\mathrm{d}\Omega}{\mathrm{d}R} = 2R\eta - 4\delta R^3,$$

which has zeros for $R_\Omega = \pm\sqrt{\frac{\eta}{2\delta}}$, indicating a change in the distortion (shear) of the phase space near the periodic orbits. At these zeros the system has radial isochrons; trajectories initialized along these radial spokes have the same asymptotic phase [37]. For $\dot{\Omega} \neq 0$ the local frequency depends on the local amplitude. We note that η and δ must have the same sign.

We define the *escape time* τ of a realization in the presence of noise as the moment at which a realization crosses a threshold between $R_{\min}$ and $R_{\max}$. Specifically,

$$\tau = \inf\{t > 0 : |z(t)| > \xi \text{ given } z(0) = 0\}, \tag{2.6}$$

where we choose the threshold $R_c \leq \xi \leq R_{\max}$. Escape time τ is a random variable that depends on the noise realization, and so we can then identify the mean escape time $T = \mathbb{E}[\tau]$. In the case of one node we can use the Eyring–Kramers formula for an asymptotic expression for T

$$T = \frac{2\pi}{\sqrt{|V''(R_c)|V''(R_{\min})}} \exp\left[\frac{2(V(R_c) - V(R_{\min})}{\alpha^2}\right] \tag{2.7}$$

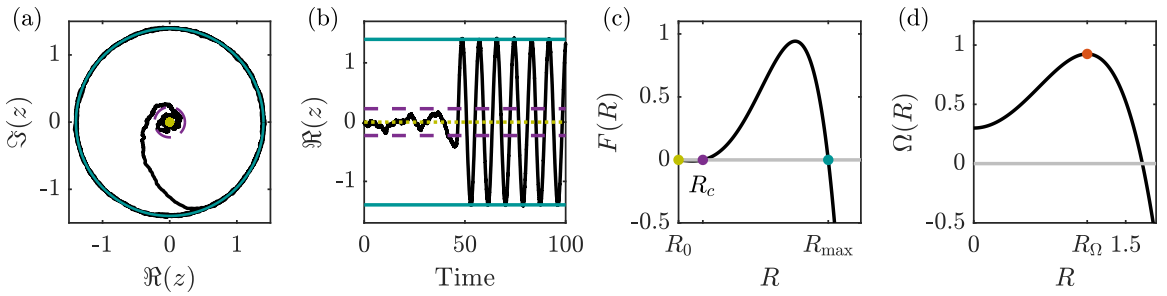

Figure 1. *Summary of one-node dynamics* (2.1) *for parameter values* (2.2). *Panels* (a) *and* (b) *show one realization of system* (2.1) *with the periodic orbits* $R_{\min} = 0$, $R_c \approx 0.23$, *and* $R_{\max} \approx 1.40$ *marked in grey. Panel* (c) *shows* (2.3a) *with periodic orbits marked at* $F(R) = 0$, *and panel* (d) *shows* (2.3b) *with* $R_\Omega \approx 1.12$ *indicating change of shear* $\mathrm{d}\Omega/\mathrm{d}R = 0$.

as $\alpha \to 0$ [10, 14]. The potential V is given by (2.5); note that V and V'' depend on α and ν but not on ω, η, or δ, and so the change of shear does not affect the escape time. A closed form expression for the mean escape time for one node with the potential described here is given in [14].

3. Sequential escapes for amplitude-only coupling. In the case that (1.1) is coupled only via amplitudes, we can express the coupling as

$$g(z_j, z_k) = G(|z_j|^2, |z_k|^2) z_k \tag{3.1}$$

and understand sequential escape dynamics purely in terms of the amplitudes only: we assume $G(0) = 0$. For simplicity, we consider fully symmetric (all-to-all) coupling so that $A_{jk} = 1$ if $j \neq k$, and $A_{jk} = 0$ otherwise. Again we consider the system in polar coordinates $z_k = R_k \exp[i\theta_k]$; then system (1.1),(1.2) with (3.1) becomes

$$\mathrm{d}R_k = \left[-\nu + 2R_k^2 - R_k^4 + \frac{\alpha^2}{2R_k} + \sum_{j \neq k} G(R_j^2, R_k^2) \right] R_k \, \mathrm{d}t + \alpha \, \mathrm{d}W_{R_k}, \tag{3.2a}$$

$$\mathrm{d}\theta_k = \left[\omega + \eta R_k^2 - \delta R_k^4 \right] \mathrm{d}t + \frac{\alpha}{R_k} \mathrm{d}W_{\theta_k}. \tag{3.2b}$$

Note that the coupling here is independent of phase dynamics as the coupling function when converted into polar coordinates only appears in the equation for R.

In the limit of low noise $0 < \alpha \ll 1$ and weak coupling $0 < |G| \ll 1$ for each unit there will be approximate equilibria at $R_k \approx 0$ and periodic orbits close to $R_k \approx R_c$ and $R_k \approx R_s$; any combination of escaped and nonescaped units is possible. However, we expect behavior somewhat different from that in [2] for increasing coupling strength. To illustrate this we consider a specific coupling function.

3.1. Symmetric nodes with amplitude-only coupling. We consider the case of N nodes with amplitude-only coupling such that $G(A_1, A_2) = cA_1A_2$ in (3.1), i.e.,

$$g(z_j, z_k) = c|z_j|^2 |z_k|^2 z_k \tag{3.3}$$

for coupling strength $c \in \mathbb{R}$. This particular form of G is chosen to ensure there is only effective coupling between active nodes.

In the noise-free case $\alpha = 0$ the zeros of

$$\frac{\mathrm{d}R_k}{\mathrm{d}t} = R_k \left[-\nu + 2R_k^2 - R_k^4 + cR_k^2 \sum_{j \neq k} R_j^2 \right] \tag{3.4}$$

correspond to families of periodic solutions of the form

$$x_{A^M Q^{N-M}} := (\rho_M e^{i(\phi_1 + \Omega_M t)}, \ldots, \rho_M e^{i(\phi_M + \Omega_M t)}, 0, \ldots, 0)$$

with M active and $N - M$ quiescent nodes and all permutations thereof; these are neutrally stable because of the absence of phase coupling. The $\rho_M > 0$ are amplitudes, ϕ_n are arbitrary constants, and the angular frequency is

$$\Omega_M := \Omega(\rho_M).$$

Note that ρ_M satisfies

$$-\nu + 2\rho_M^2 + [-1 + c(M-1)]\rho_M^4 = 0,$$

and so the amplitude of the oscillations will increase (or decrease) with the number of escaped nodes, depending on the sign of c. We can solve this to give

$$\rho_M^{\pm} = \sqrt{\frac{1 \pm \sqrt{1 - \nu + \nu c(M-1)}}{1 - c(M-1)}}. \tag{3.5}$$

Recall that $0 < \nu < 1$ so that the uncoupled systems are bistable. For $M = 1$ escaped state (active node) we retrieve $\rho_1^+ = R_{\max}$ and $\rho_1^- = R_c$ shown in Figure 1. From (3.5) we find that solutions x_{A^3} exist for $-4.5 < c < 0.5$, solutions $x_{A^2Q^1}$ exist for $-9 < c < 1$, and solutions $x_{A^1Q^2}$ exist for all c. Note that the stability of solutions may change with c, and this is not captured by (3.5). To illustrate this, the full picture of (3.4) for the specific example using $N = 3$ and $\nu = 0.1$ is shown in Figure 2; we plot the bifurcation diagram of R_1 against c. We identify additional bifurcations corresponding to changes in stability of solutions for $c \approx -0.8$. This implies that, similar to [2, 14], we will have a weak coupling regime.

More generally, the decoupling of the phase dynamics means that starting from the fully inactive state x_{Q^N}, several scenarios of sequential escapes are possible varying c.

- For small $c > 0$, successive escapes will result in active oscillatory states with larger amplitude. We expect an *accelerating domino* transition as the basin to escape from becomes successively shallower.
- For $c \gg 0$, if
$$M_{c^+} = \min\{M \in \mathbb{N} \ : \ c(M-1) > 1\},$$
then all partially escaped states $\rho_M^{\pm}$ for $M \geq M_{c^+}$ will be unstable, and so we expect very fast noise-driven escapes from the M_{c^+}th to the Nth.
- For small $c < 0$, successive escapes will result in smaller amplitude active oscillations. We expect a *decelerating domino* transition where successive escapes become slower as the basin to escape from becomes successively deeper.

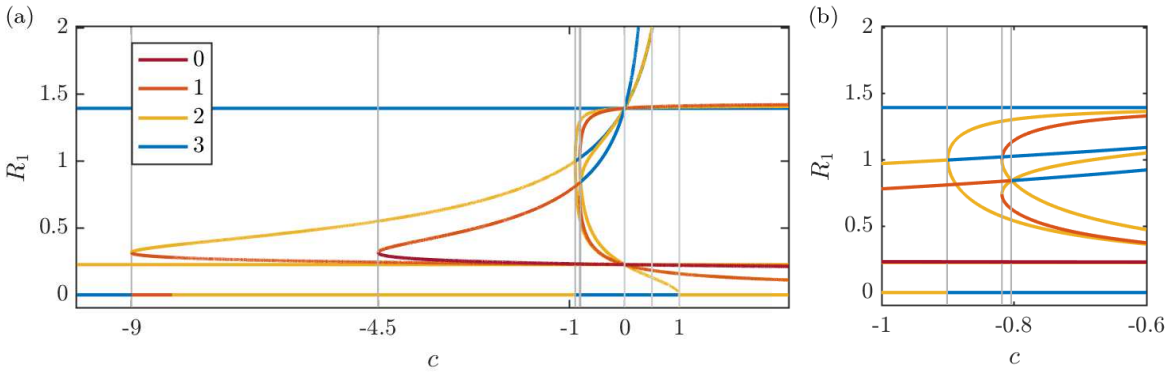

Figure 2. *Bifurcation diagram for three node-system* (3.2a) *with* (3.3) *for* $\alpha = 0$ *and* $\nu = 0.1$ *projected onto the* (R_1, c)*-plane. Panel* (a) *shows the full bifurcation diagram in* R_1 *and* c*. The legend indicates the number of stable eigenvalues of the equilibria. The lines of existence of solutions elucidated from* (3.5) *are shown in grey at* $c = \{-9, -4.5, 0.5, 1\}$*;* $c = 0$ *is also marked. Panel* (b) *shows an enlargement around* $c = -0.8$*. Bifurcations are marked by grey lines; there is a saddle node bifurcation at* $c = -0.8182$*, a pitchfork bifurcation at* $c = -0.9$*, and a transverse pitchfork at* $c = -0.8034$*.*

- For $c \ll 0$, if
$$M_{c^-} = \min\{M \in \mathbb{N} \ : \ |c|(M-1) > 1 - \nu\},$$
then there are no solutions $\rho_M^{\pm}$ for $M \leq M_{c^-}$, and in this case the sequence will terminate before all nodes have escaped.

We illustrate the accelerating or decelerating domino effect by numerically computing the escape times for the three-node system (1.1),(1.2) with (3.1). For a given threshold ξ we compute the escape time of the ith node

$$\tau^{(i)} = \inf\{t > 0 : |z_i(t)| > \xi \text{ given } z_i(0) = 0\}. \tag{3.6}$$

The random variable $\tau^{(i)}$ depends on ξ, the noise realization, and the influence from other nodes. We choose ξ to contain the whole basin of attraction of solution starting at $z = 0$ [6]. To this end we use $\xi = 0.75$; Figure SM1 in the supplementary material shows that this is larger than ρ_M^- for all M in the weak coupling regime considered here $c = [-0.6, 0.6]$. For a fixed threshold the independence of the noise processes W means that no two escapes will occur at precisely the same time, so we can assume an ordering $s(i)$ from 1 to 3 in this three-node example. We define the ith escape as $\tau^i := \tau^{(s(i))}$ and the escape time of the kth node given that $k-1$ nodes have escaped as $\tau^{k|k-1} = \tau^k - \tau^{k-1}$ for integers $0 < k \leq 3$. The mean conditional escape time is $T^{k|k-1} = \mathbb{E}[\tau^{k|k-1}]$. Here we compute the mean conditional escape times for the first, second, and third escapes over 1000 realizations of the system computed using the stochastic Heun method.

Figure 3 shows the distributions and means of the conditional escape times for values of c in the weak coupling regime. This figure illustrates the accelerating and decelerating domino effect. Note that although the scale changes in each panel of row (a), the distributions of the first conditional escape time $\tau^{1|0}$ are similar for all c. The distributions of the second $\tau^{2|1}$

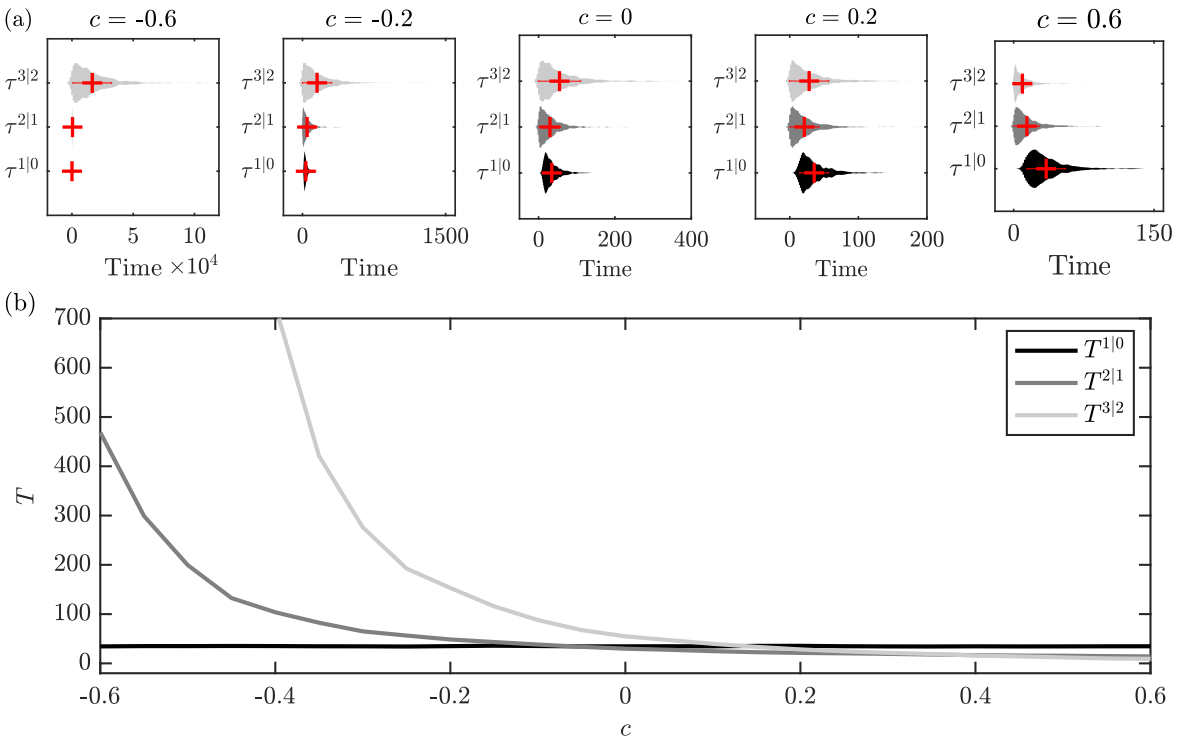

Figure 3. *Distributions of conditional escape times of a three-node system with amplitude-only coupling for different values of coupling strength c. Each distribution was computed using* 1000 *realizations. This illustrates that in the weak coupling regime, for $c > 0$ the domino effect accelerates, whereas for $c < 0$ the domino effect decelerates.*

and third $\tau^{3|2}$ conditional escape times become narrower in time for $c > 0$, and their mean conditional escape times decrease below $T^{1|0}$. For $c < 0$ the distributions of $\tau^{2|1}$ and $\tau^{3|2}$ cover a longer time period than for $c = 0$, and the mean conditional escape times increase exponentially. Example realizations for fixed values of c are shown in Figures SM2–SM3 of the supplementary material.

Note that if we look at escape from M to $M+1$, then we pass saddles of the form

$$(\rho_M e^{i(\phi_1+\Omega_1 t)}, \ldots, \rho_M e^{i(\phi_M+\Omega_1 t)}, \sigma_M e^{i(\phi_{M+1}+\Omega_2 t)}, 0, \ldots, 0),$$

where ρ_M (we omit the $\pm$ for ease of notation) and σ_M need to be computed as solutions of a quartic equation. As above, the ϕ_i are constants, and $\Omega_1 = \Omega(\rho_M)$, $\Omega_2 = \Omega(\sigma_M)$. Observe that typically, Ω_1 and Ω_2 are incommensurable, meaning these "gates" will typically consist of invariant tori.

4. Sequential escapes for phase-amplitude coupling. We now consider a case where system (1.1),(1.2) can show nontrivial phase dynamics, for N amplitude coupled nodes, modified by phase-dependent coupling,

$$g(z_j, z_k) = \varepsilon e^{i\psi}|z_k|^2 z_j + c|z_j|^2|z_k|^2 z_k, \tag{4.1}$$

where $\varepsilon \geq 0$ and ψ modulate the strength and relative phase of the linear diffusive coupling. Note that we consider multiplicative coupling to ensure that the coupling does not substantially affect the quiescent states. In this section we investigate the effects on the phase and timings of sequential escapes of the network when changing ε and c and keeping ψ fixed.

As before, we consider an all-to-all fully symmetric network, i.e., $A_{jk} = 1$ if $j \neq k$, and $A_{jk} = 0$ otherwise. Using Ito's formula we write system (1.1),(1.2),(4.1) in polar coordinates $z_k(t) = R_k(t)\exp[i\theta_k(t)]$ for $k = 1, \ldots, N$ as

$$\mathrm{d}R_k = \left[F(R_k) + \varepsilon\Big(\sum_{j\neq k} R_k^2 R_j \cos(\psi + \theta_{jk})\Big) + c\sum_{j\neq k} R_j^2 R_k^3 + \frac{\alpha^2}{2R_k}\right]\mathrm{d}t + \alpha \mathrm{d}W_{R_k}, \tag{4.2a}$$

$$\mathrm{d}\theta_k = \left[\Omega(R_k) + \varepsilon\Big(\sum_{j\neq k} R_j R_k \sin(\psi + \theta_{jk})\Big)\right]\mathrm{d}t + \frac{\alpha}{R_k}\mathrm{d}W_{\theta_k}, \tag{4.2b}$$

where $\mathrm{d}W_{R_k}$ and $\mathrm{d}W_{\theta_k}$ are independent real valued Wiener processes, and $\theta_{jk} := \theta_j - \theta_k$. Note here that the coupling modulates the frequency and the amplitude of the nodes.

4.1. Symmetric nodes with weak phase dynamics. For typical choices of parameters where there are stable limit cycles, (4.2a),(4.2b) can be reduced in the case of $\alpha = 0$ (noise-free) and $\varepsilon \ll 1$ (weak phase coupling) [22]. To consider solutions near $x_{A^M Q^{N-M}}$, we write

$$R_k = \begin{cases} \rho_M + \varepsilon r_k & \text{for } k = 1, \ldots, M, \\ \varepsilon r_k & \text{for } k = M+1, \ldots, N. \end{cases}$$

As before, the amplitude of the stable limit cycle in the amplitude-only coupled (i.e., in c only) case $\varepsilon = 0$ is ρ_M. Expanding (4.2a) about this solution to first order in ε, we have for $k = 1, \ldots, M$ that

$$\frac{\mathrm{d}}{\mathrm{d}t} r_k = F'_M r_k + \sum_{j=1,\neq k}^{M} \left[\rho_M^3 \cos(\psi + \theta_{jk}) + 2c\rho_M^4 r_j\right] + Mc\rho_M^4 r_k + O(\varepsilon), \tag{4.3}$$

where $F'_M = F'(\rho_M)$.

If we define $\overline{r} = \sum_{j=1}^{M} r_j$, then by adiabatic elimination,

$$r_k = \frac{2c\rho_M^4 \overline{r} + \rho_M^3 \sum_{j=1,\neq k}^{M} [\cos(\psi + \theta_{jk})]}{F'_M + (3M-2)c\rho_M^4} + O(\varepsilon). \tag{4.4}$$

Summing this over $k = 1, \ldots, M$ gives

$$\overline{r} = \frac{2Mc\rho_M^4 \overline{r} + 2\rho_M^3 \sum_{k=1}^{M} \sum_{j<k} [\cos(\psi)\cos(\theta_{jk})]}{F'_M + (3M-2)c\rho_M^4} + O(\varepsilon),$$

which can be solved to give

$$\overline{r} = \frac{2\rho_M^3 \cos(\psi) \sum_{k=1}^{M} \sum_{j<k} \cos(\theta_{jk})}{F'_M + (M-2)c\rho_M^4} + O(\varepsilon). \tag{4.5}$$

Substituting (4.5) into (4.4), we have

$$r_k = H(\theta) + h_k(\theta) + O(\varepsilon), \tag{4.6}$$

which gives r_k in terms of angles, where

$$H(\theta) := \frac{2c\rho_M^4}{F'_M + (3M-2)c\rho_M^4} \frac{2\rho_M^3 \cos(\psi) \sum_{k=1}^{M} \sum_{j<k} \cos(\theta_{jk})}{F'_M + (M-2)c\rho_M^4}$$

and

$$h_k(\theta) := \frac{\rho_M^3 \sum_{j=1,\neq k}^{M} [\cos(\psi + \theta_{jk})]}{F'_M + (3M-2)c\rho_M^4}.$$

Similarly, substituting $R_k = \rho_M + \varepsilon r_k$ into (4.2b) with $\alpha = 0$ gives phase equations

$$\frac{\mathrm{d}}{\mathrm{d}t}\theta_k = \Omega_M + \varepsilon \left[\Omega'_M r_k + \sum_{j \neq k} \rho_M^2 \sin(\psi + \theta_{jk}) \right] + O(\varepsilon^2) \tag{4.7}$$

for $k = 1, \ldots, M$ where $\Omega'_M := \Omega'(\rho_M)$, and so

$$\frac{\mathrm{d}}{\mathrm{d}t}\theta_k = \Omega_M + \varepsilon \left[\Omega'_M \left[H(\theta) + h_k(\theta) \right] + l_k(\theta) \right] + O(\varepsilon^2) \tag{4.8}$$

and

$$l_k(\theta) := \sum_{j \neq k} \rho_M^2 \sin(\psi + \theta_{jk}).$$

This can be used, in principle, to calculate the stability of a variety of solutions, including in-phase and splay phase oscillations; see, for example, (4.11).

4.2. Phase synchrony during escape. The nontrivial phase dynamics can be observed in system (1.1),(1.2) with (4.1) for $N \geq 3$ nodes. We show example realizations of $N = 3$ nodes with weak amplitude coupling $-0.2 < c < 0.2$ for $\varepsilon > 0$ in Figure 4 and for $\varepsilon < 0$ in Figure 5. Here we fix the parameters

$$\nu = 0.1,\ \omega = 0.3,\ \eta = 1.0,\ \delta = 0.4,\ \alpha = 0.035,\ \psi = \pi/2. \tag{4.9}$$

For each set of c and ε values, we compute the order parameter

$$\pi^{1,\ldots,N_e}(t) = \frac{\left| \sum_{k=1}^{N_e} \exp^{i\theta_k(t)} \right|}{N_e}, \tag{4.10}$$

where $N_e > 1$ is the number of escaped nodes in a given realization. Specifically, when $N_e = 2$, $\pi^{1,2}(t)$ is the order parameter computed between the first and second nodes to escape. When $\pi = 1$ the nodes are synchronized, and when $\pi = 0$ the nodes are antisynchronous. Due to the large fluctuations in synchrony between nodes before escape we do not compute $\pi(t)$ at the moment of escape. To capture the phase dynamics of the escapes numerically we compute $\pi^{1,2}(t^{(2)})$ at time point $t^{(2)} = \tau^2 + \frac{\tau^3 - \tau^2}{2}$ between the second and third escape times (as

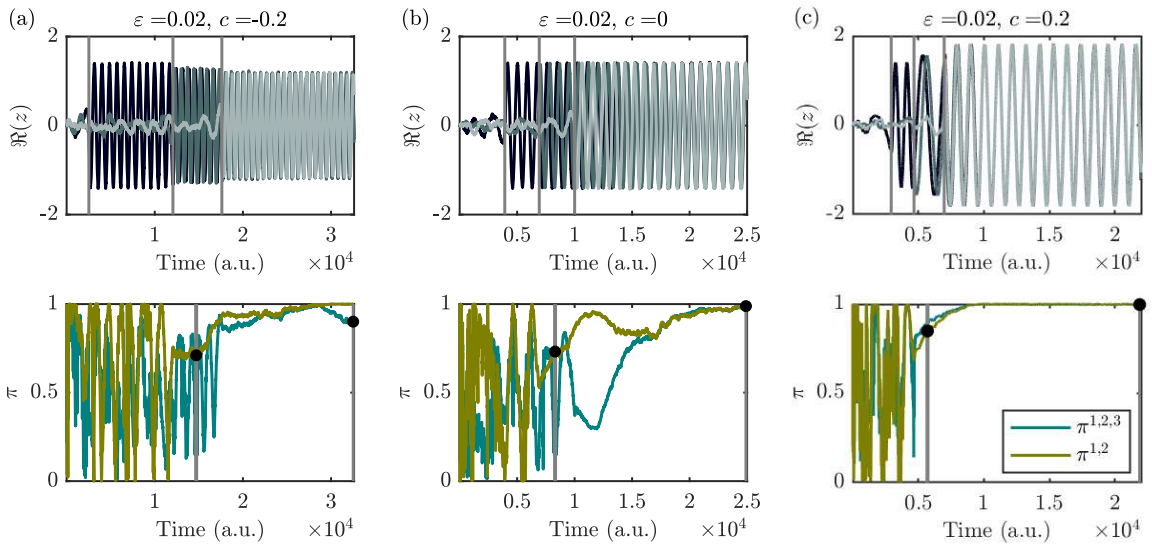

Figure 4. *Examples of sequential escapes for $N = 3$ oscillators with coupling (4.1) and parameters (4.9) for $\varepsilon = 0.02$ and $c = -0.2$ (a), $c = 0$ (b), and $c = 0.2$ (c). The top row shows the real component of z for each node plotted against time in arbitrary units (a.u.); note that nodes are colored by order of escape, and the precise times of escape are determined by details of the noise. The bottom row shows the order parameter between the first two nodes to escape $\pi^{1,2}(t)$ (olive) and all three nodes $\pi^{1,2,3}(t)$ (teal). The black dots on each curve denote the phase points $\pi^{1,2}(t^{(2)})$ and $\pi^{1,2,3}(t^{(3)})$, respectively. Note that $\pi^{1,2,3}(t^{(3)}) > \pi^{1,2}(t^{(2)})$ and that nodes tend to synchrony when all have escaped $\pi^{1,2,3}(t^{(3)}) \approx 1$.*

defined in section 3.1), and we compute $\pi^{1,2,3}(t^{(3)})$ at $t^{(3)} = \tau^3 + 1.5 \times 10^4$ after the third escape. Example realizations shown in Figures 4 and 5 are computed using the stochastic Heun method with step size $h = 10^{-2}$ and a different seed for the random process each time. Figure 4 shows that for $\varepsilon = 0.02 > 0$, realizations tend to synchrony between escaped nodes, whereas Figure 5 shows that realizations tend to antisynchrony for $\varepsilon = -0.02 < 0$. In the case $\varepsilon = 0$ there is amplitude-only coupling as described in section 3.1. Therefore the amplitude of the escaped solutions changes, but synchrony between nodes does not change with the escapes; example realizations for $\varepsilon = 0$ are shown in Figure SM4 of the supplementary material.

As in section 3.1 we compute numerically the mean conditional escape times $T^{1|0}$, $T^{2|1}$, and $T^{2|3}$ of the system. In the same way, we note that the order parameter π is a random variable that depends on the noise realization and the coupling. We define the mean order parameter $P^{1,\dots,N_e} = \mathbb{E}[\pi^{1,\dots,N_e}(t^{(N_e)})]$ as the expectation of the order parameter at one time point $t^{(N_e)}$. We numerically approximate $P^{1,\dots,N_e}$ for $N_e = 2$ and $N_e = 3$ by taking the mean of the order parameter at time points $t^{(2)}$ and $t^{(3)}$, respectively, computed from 1000 realizations using the Heun method as above.

Figure 6 shows the mean escape times $T^{1|0}$, $T^{2|1}$, and $T^{2|3}$ and mean order parameters $P^{1,2}$ and $P^{1,2,3}$ for parameters (4.9), $c \in [-0.2, 0.2]$, and $\varepsilon \in [-0.02, 0.02]$. Note that the mean escape times T (left axis) are unaffected by changes in ε and follow the dependence on c shown in Figure 3(b). By comparison the mean order parameter for two escaped nodes $P^{1,2}$

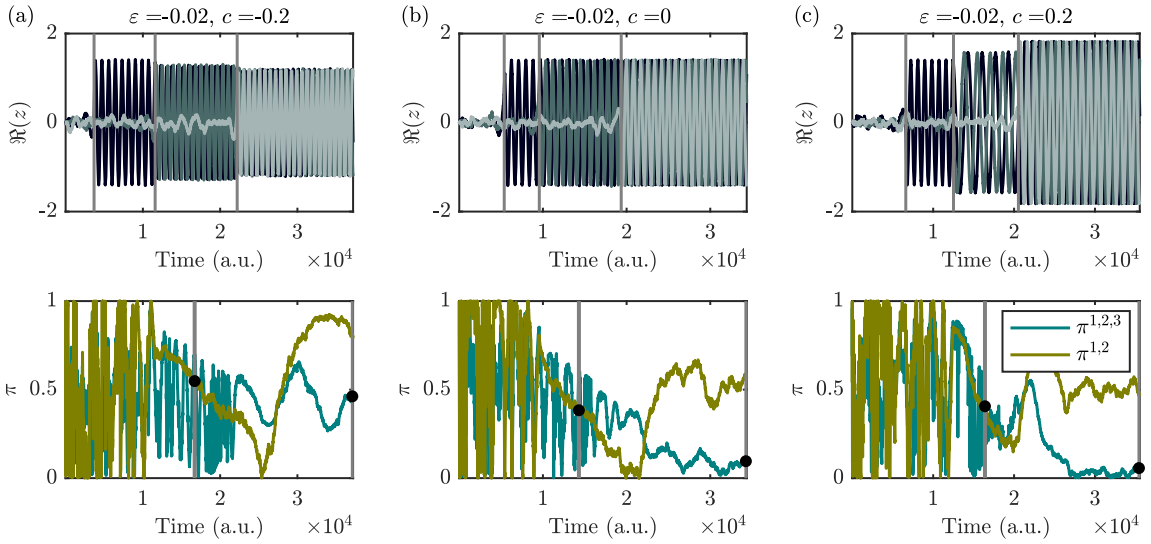

Figure 5. *Examples of sequential escapes for $N = 3$ oscillators with coupling (4.1) and parameters (4.9) for $\varepsilon = -0.02$ and $c = -0.2$ (a), $c = 0$ (b), and $c = 0.2$ (c); compare to Figure 4. The top row shows the real component of z for each node; the bottom row shows the order parameter between the first two nodes to escape $\pi^{1,2}(t)$ (olive) and all three nodes $\pi^{1,2,3}(t)$ (teal). The black dots on each curve denote the phase points $\pi^{1,2}(t^{(2)})$ and $\pi^{1,2,3}(t^{(3)})$, respectively. Note that $\pi^{1,2}(t^{(2)})$ is similar for all c and and that when all nodes have escaped for $c \geq 1$ they tend to antisynchrony $\pi^{1,2,3}(t^{(3)}) \approx 0$ for $c \geq 0$.*

remains relatively constant for each ε value and is not influenced by the amplitude coupling c, whereas the mean order parameter for three escaped nodes $P^{1,2,3}$ displays dependence on both c and ε. Compare the values of $P^{1,2}$ and $P^{1,2,3}$ to the points $\pi^{1,2}(t^{(2)})$ and $\pi^{1,2,3}(t^{(3)})$ in Figures 4 and 5.

4.3. Example of changes in synchrony during escape. Note that (4.8) can be used to find the stability of the in-phase partially escaped state for $M \geq 2$. Consider perturbations of the form $\theta_1 = \Theta + \Delta$, $\theta_k = \Theta$ for $k = 2, \ldots, M$ and note that

$$\begin{aligned}\frac{\mathrm{d}}{\mathrm{d}t}\Delta &= \frac{\mathrm{d}}{\mathrm{d}t}[\theta_1 - \theta_k] \\ &= \varepsilon\left[\Omega'_M\left[h_1(\theta) - h_k(\theta)\right] + l_1(\theta) - l_k(\theta)\right].\end{aligned}$$

For illustration we choose $\psi = \frac{3\pi}{2}$, such that $H(\theta) = 0$ and $h_k(\theta) = D\rho_M^3 \sum_{j=1,\neq k}^{M} \sin(\theta_{jk})$, where

$$D := \frac{1}{F'_M + (3M-2)c\rho_M^4},$$

and $l_k(\theta) = -\rho_M^2 \sum_{j\neq k} \cos(\theta_{jk})$. Then

$$\frac{\mathrm{d}}{\mathrm{d}t}\Delta = \varepsilon\left[-M\Omega'_M D\rho_M^3 \sin\Delta + \rho_M^2\left[(M-2)(\cos\Delta - 1)\right]\right]. \tag{4.11}$$

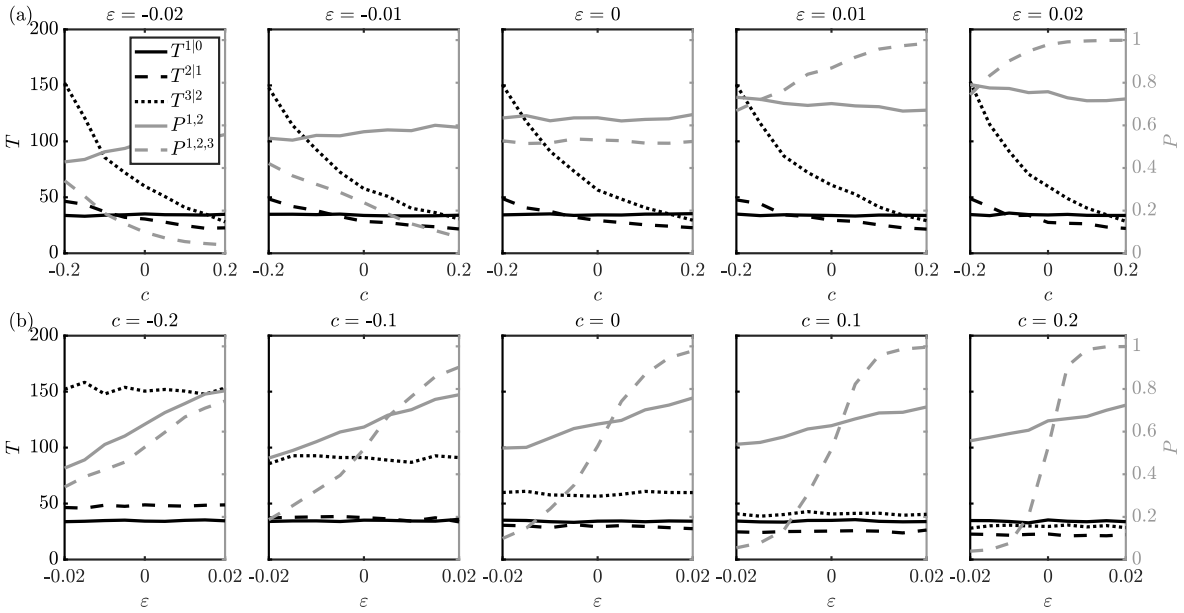

Figure 6. *The mean conditional escape times $T^{k|k-1}$ and mean order parameter $P^{1,\dots,N_e}$ for different values of c with fixed ε* (a) *and different values of ε for fixed c* (b). *The mean first $T^{1|0}$, second $T^{2|1}$, and third $T^{3|2}$ conditional escape times are shown in black, and the mean order parameter between the first and second nodes to escape $P^{1,2}$ and between all three nodes $P^{1,2,3}$ after the third escape are shown in grey. Each point is the mean over* 1000 *simulations.*

If we linearize this about the in-phase state $\Delta = 0$, then we find

$$\frac{\mathrm{d}}{\mathrm{d}t}\Delta = -\varepsilon M \Omega'_M D \rho_M^3 \Delta + O(\Delta^3), \tag{4.12}$$

which means that for small $\varepsilon > 0$ the stability of the in-phase solution is determined at this order of truncation as long as $\Omega'_M D$ is nonzero, and stability is determined by the sign of this quantity. In particular, note that a change in the sign of Ω'_M as M increases will be associated with changes in stability of in-phase synchrony as a sequence of escapes progresses. Figure 7 illustrates this change in sign of Ω'_M for $M = 2, 3$ for the three-node network example. In particular, for $c = \{-0.2, 0, 0.2\}$, amplitudes $\rho_M^{\pm} > R_\Omega$ such that $\Omega'(\rho_M^+) < 0$ for $M = 2, 3$. At $c \approx -0.268$, $\rho_3^{\pm} = R_\Omega$, and for $c = -0.4$, $\Omega'(\rho_2^+) < 0$ and $\Omega'(\rho_3^+) > 0$, indicating a change of cluster synchrony between escapes. Finally, $\rho_2^{\pm} = R_\Omega$ at $c \approx -0.536$, and for $c = -0.6$, $\Omega'(\rho_M^+) > 0$ for $M = 2, 3$.

Changes in cluster synchrony can be observed in the realizations for $c = -0.4$ shown in Figure 8. In particular, $\varepsilon < 0$ gives stable antisynchrony of two escaped oscillators which is replaced by stable synchrony for three escaped oscillators. Using the same parameters but reversing the sign of $\varepsilon > 0$, the second escape shows stable synchrony for two escaped oscillators, but the third escape shows stable antisynchrony for the three escaped oscillators. We note that this change of sign can be achieved instead via shifting $R(\Omega)$ by altering η and δ, as shown in Figure SM5 of the supplementary material. In this case the change of synchrony

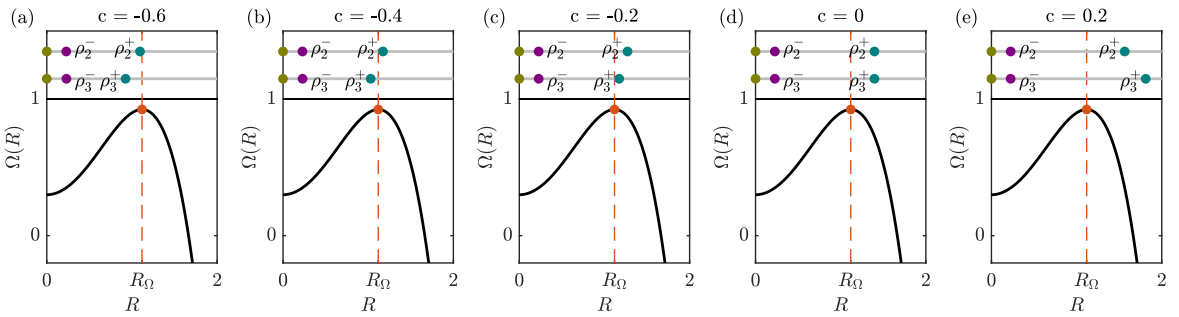

Figure 7. *Graphs of* $\Omega(R)$ *given by* (2.4b) *with amplitudes* $\rho_M^\pm$ *given by* (3.5). *For* $c = -0.6$ *in panel* (a), *gradients* $\Omega'(\rho_M^+) > 0$ *for* $M = 2, 3$. *In panel* (b), $c = -0.4$ *such that* $\Omega'(\rho_2^+) < 0$ *and* $\Omega'(\rho_3^+) > 0$. *In panels* (c)–(e), $c \geq -0.2$ *and* $\Omega'(\rho_M^+) < 0$ *for* $M = 2, 3$. *The critical values of* c *are* $\rho_3^+ = R_\Omega$ *for* $c \approx -0.268$ *and* $\rho_3^+ = R_\Omega$ *for* $c \approx -0.536$.

is not as pronounced. We show the distributions of the conditional escape times shown in Figure 8 and the order parameters in Figure SM6 of the supplementary material.

5. Discussion. In this paper we investigate the link between synchrony and sequential escapes and characterize this in terms of the mean order parameter between escaped nodes and of the mean time between consecutive escapes. The model of sequential escapes we consider here is an idealized model of coupled systems with bistability between a stable quiescent equilibrium and a stable active periodic state. The form of coupling we choose allows us to control coupling dynamics via amplitude and phase of the oscillations. Furthermore, it is of a sufficiently simple form that one can perform an analysis of synchrony for the partially escaped states. For more realistic, physically motivated models it is unlikely that this analysis is possible, but nonetheless we expect qualitative behaviors, such as changes of synchrony along a sequence of escapes, to still be present.

A classical approach to coupled oscillator theory is to consider only the phase effects and reduce the system to coordinates that parameterize the limit cycle. In the case of weak coupling, phenomena such as phase locking are well documented [25, 15]. However, when the attraction to the limit cycle is weak, such as near a Hopf bifurcation, it is no longer possible to assume that trajectories stay with epsilon of the limit cycle, and the amplitude must be taken into account. Aronson, Ermentrout, and Kopell [1] discuss the effect of shear in symmetrically coupled oscillators near a Hopf bifurcation. They show that for two identical oscillators with nonscalar coupling there is bistability of asymptotically stable phase-locked and phase-drift solutions. We extend this idea for three nodes with phase-amplitude coupling to a noisy context and illustrate how shear relates to the appearance of transient synchronous and antisynchronous solutions between sequential escapes.

We make some additional remarks on the influence of α (noise level), ε (phase coupling strength), and c (amplitude coupling strength) on the mean escape time T_e and the constant T_s characterizing exponential decay towards a stable synchronous/antisynchronous state. In the tractable limit considered here (where all α, ε, and c are small), T_e is approximated by Kramers' formula (2.7), namely $T_e \sim \exp(K/\alpha^2)$, with $K > 0$ the height of the potential

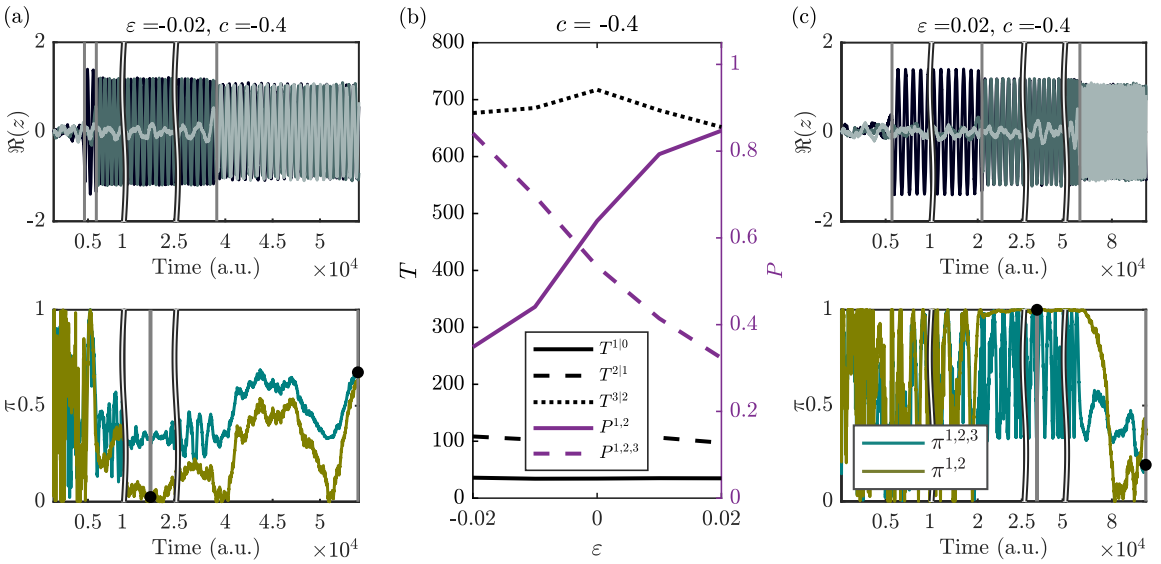

Figure 8. *Synchrony changes during sequential escape of $N = 3$ oscillators with coupling (4.1) for $c = -0.4$. Panel* (b) *shows the mean escape times T (black, left axis) and mean order parameter P (purple, right axis) for different values of $\varepsilon \in [-0.02, 0.02]$; compare to Figure 6*(b)*. Panels* (a) *and* (c) *shows example realizations (top) for $\varepsilon = -0.02$ and $\varepsilon = 0.02$, respectively, with the order parameters (bottom) $\pi^{1,2}(t)$ (olive) and $\pi^{1,2,3}(t)$ (teal). Note that the time-axis contains breaks to aid visualization. The points $\pi^{1,2}(t^{(2)})$ and $\pi^{1,2,3}(t^{(3)})$ are marked as black dots, showing the change from antisynchrony after the second escape to synchrony after the third escape in* (a) *and from synchrony after the second escape to antisynchrony after the third escape in* (c).

barrier to be overcome, while T_s is approximated by the reciprocal of the linear coefficient in (4.12), i.e., $T_s \sim 1/\varepsilon$. Hence for small c, in order to expect that transient synchronous behavior settles to a stable state before the next escape occurs, we need $T_s \ll T_e$. This means we will expect to see the transient synchrony fully realized in cases where $\exp(-K/\alpha^2) \ll \varepsilon$. It would be interesting to better understand this interplay between timescales of escape and timescales of transition to synchrony. This would require further analysis of the temporal evolution of the order parameter over the timescale of the escape time dynamics.

Although we do not consider applications in this paper, there is a clear implication that sequential escapes in systems of coupled oscillators can be associated with a wide variety of changes in synchrony. In particular, it is possible that transitions from quiescent states to active states may give strong signals in the mean field only for certain states in the sequence. We note that the instantaneous synaptic coupling term commonly used in biophysical models is nonlinear due to the sigmoidal function nature of the gating variable. If one considers a linearization of the gating function, then the instantaneous synaptic coupling term would look very much like what we have in this article, provided that the synaptic reversal potential is equal to 0. Phase-amplitude coupling has been recently recognized as important in brain dynamics and, more specifically, information processing [11]. Using dynamic causal modeling, Fagerholm et al. [17] quantify the separate contributions of phase and amplitude to the connectivity between neural regions. For seizure onset and progression in epilepsy,

our work aligns with experimental evidence indicating that seizures result from the dynamic interactions between neuronal networks characterized by an evolving degree of heterogeneity in neuronal firing. Specifically, desynchronization has been shown to precede seizures or found during their early stages, while in contrast, high levels of synchronization have been observed before seizures terminate [24, 28], reminiscent of the simulations depicted in Figure 4(a).

REFERENCES

[1] D. G. Aronson, G. B. Ermentrout, and N. Kopell, *Amplitude response of coupled oscillators*, Phys. D, 41 (1990), pp. 403–449.

[2] P. Ashwin, J. Creaser, and K. Tsaneva-Atanasova, *Fast and slow domino regimes in transient network dynamics*, Phys. Rev. E, 96 (2017), 052309.

[3] P. Ashwin, J. Creaser, and K. Tsaneva-Atanasova, *Sequential escapes: Onset of slow domino regime via a saddle connection*, Eur. Phys. J. Special Topics, 227 (2018), pp. 1091–1100.

[4] A. K. al Azad and P. Ashwin, *Within-burst synchrony changes for coupled elliptic bursters*, SIAM J. Appl. Dynam. Syst., 9 (2010), pp. 261–281, https://doi.org/10.1137/090746045.

[5] O. Benjamin, T. H. Fitzgerald, P. Ashwin, K. Tsaneva-Atanasova, F. Chowdhury, M. P. Richardson, and J. R. Terry, *A phenomenological model of seizure initiation suggests network structure may explain seizure frequency in idiopathic generalised epilepsy*, J. Math. Neurosci., 2 (2012), pp. 1–30.

[6] N. Berglund and B. Gentz, *Noise-Induced Phenomena in Slow-Fast Dynamical Systems: A Sample-Paths Approach*, Springer Science+Business Media, 2006.

[7] N. Berglund, B. Fernandez, and B. Gentz, *Metastability in interacting nonlinear stochastic differential equations* I: *From weak coupling to synchronization*, Nonlinearity, 20 (2007), pp. 2551–2581.

[8] N. Berglund, B. Fernandez, and B. Gentz, *Metastability in interacting nonlinear stochastic differential equations* II: *Large-n behaviour*, Nonlinearity, 20 (2007), pp. 2583–2614.

[9] N. Berglund and B. Gentz, *The Eyring-Kramers' Law for Potentials with Nonquadratic Saddles*, preprint, http://arxiv.org/abs/0807.1681, 2008.

[10] N. Berglund, *Kramers' law: Validity, derivations and generalisations*, Markov Process. Related Fields, 19 (2013), pp. 459–490.

[11] T. O. Bergmann and J. Born, *Phase-amplitude coupling: A general mechanism for memory processing and synaptic plasticity?*, Neuron, 97 (2018), pp. 10–13.

[12] M. Chávez, M. Le Van Quyen, V. Navarro, M. Baulac, and J. Martinerie, *Spatio-temporal dynamics prior to neocortical seizures: Amplitude versus phase couplings*, IEEE Trans. Biomed. Engrg., 50 (2003), pp. 571–583.

[13] F. Clément and J.-P. Françoise, *Mathematical modeling of the GnRH pulse and surge generator*, SIAM J. Appl. Dyn. Syst., 6 (2007), pp. 441–456, https://doi.org/10.1137/060673825.

[14] J. Creaser, K. Tsaneva-Atanasova, and P. Ashwin, *Sequential noise-induced escapes for oscillatory network dynamics*, SIAM J. Appl. Dyn. Syst., 17 (2018), pp. 500–525, https://doi.org/10.1137/17M1126412.

[15] G. B. Ermentrout, *n:m phase-locking of weakly coupled oscillators*, J. Math. Biol., 12 (1981), pp. 327–342.

[16] H. Eyring, *The activated complex in chemical reactions*, J. Chem. Phys., 3 (1935), pp. 107–115.

[17] E. D. Fagerholm, R. J. Moran, I. R. Violante, R. Leech, and K. J. Friston, *Dynamic causal modelling of phase-amplitude interactions*, NeuroImage, 208 (2020), 116452.

[18] S. Fernández-García, M. Desroches, M. Krupa, and F. Clément, *A multiple time scale coupling of piecewise linear oscillators: Application to a neuroendocrine system*, SIAM J. Appl. Dyn. Syst., 14 (2015), pp. 643–673, https://doi.org/10.1137/140984464.

[19] K. D. Harris and A. Thiele, *Cortical state and attention*, Nature Rev. Neurosci., 12 (2011), pp. 509–523.

[20] L. Higginbotham, L. Trotti, D. Bliwise, and S. Miocinovic, *Cortical phase amplitude coupling and pathologic synchronization during sleep in Parkinson's disease*, Neurology, 92 (2019), S10.004.

[21] D. Holcman and M. Tsodyks, *The emergence of up and down states in cortical networks*, PLoS Comput. Biol., 2 (2006), e23.
[22] E. M. Izhikevich, *Dynamical Systems in Neuroscience*, MIT Press, 2007.
[23] D. Jercog, A. Roxin, P. Bartho, A. Luczak, A. Compte, and J. De La Rocha, *Up-down cortical dynamics reflect state transitions in a bistable network*, Elife, 6 (2017), e22425.
[24] P. Jiruska, M. De Curtis, J. G. Jefferys, C. A. Schevon, S. J. Schiff, and K. Schindler, *Synchronization and desynchronization in epilepsy: Controversies and hypotheses*, J. Physiol., 591 (2013), pp. 787–797.
[25] N. Kopell and G. Ermentrout, *Symmetry and phaselocking in chains of weakly coupled oscillators*, Comm. Pure Appl. Math., 39 (1986), pp. 623–660.
[26] H. A. Kramers, *Brownian motion in a field of force and the diffusion model of chemical reactions*, Physica, 7 (1940), pp. 284–304.
[27] A. Luczak, P. Barthó, S. L. Marguet, G. Buzsáki, and K. D. Harris, *Sequential structure of neocortical spontaneous activity in vivo*, Proc. Natl. Acad. Sci. USA, 104 (2007), pp. 347–352.
[28] K. Majumdar, P. D. Prasad, and S. Verma, *Synchronization implies seizure or seizure implies synchronization?*, Brain Topography, 27 (2014), pp. 112–122.
[29] H. Malchow, W. Ebeling, R. Feistel, and L. Schimansky-Geier, *Stochastic bifurcations in a bistable reaction-diffusion system with Neumann boundary conditions*, Ann. Phys., 495 (1983), pp. 151–160.
[30] R. Milton, N. Shahidi, and V. Dragoi, *Dynamic states of population activity in prefrontal cortical networks of freely-moving macaque*, Nature Comm., 11 (2020), 1948.
[31] A. Neiman, *Synchronization-like phenomena in coupled stochastic bistable systems*, Phys. Rev. E, 49 (1994), pp. 3484–3487.
[32] A. Pérez-Cervera, P. Ashwin, G. Huguet, T. M. Seara, and J. Rankin, *The uncoupling limit of identical Hopf bifurcations with an application to perceptual bistability*, J. Math. Neurosci., 9 (2019), pp. 1–33.
[33] S. Röblitz, C. Stötzel, P. Deuflhard, H. M. Jones, D.-O. Azulay, P. H. van der Graaf, and S. W. Martin, *A mathematical model of the human menstrual cycle for the administration of GnRH analogues*, J. Theoret. Biol., 321 (2013), pp. 8–27.
[34] A. Sherman, *Anti-phase, asymmetric and aperiodic oscillations in excitable cells – I: Coupled bursters*, Bull. Math. Biol., 56 (1994), pp. 811–835.
[35] R. C. Sotero, *Modeling the generation of phase-amplitude coupling in cortical circuits: From detailed networks to neural mass models*, BioMed Res. Int., 2015 (2015), 915606.
[36] M. Steriade, A. Nunez, and F. Amzica, *A novel slow (<1 Hz) oscillation of neocortical neurons in vivo: Depolarizing and hyperpolarizing components*, J. Neurosci., 13 (1993), pp. 3252–3265.
[37] A. T. Winfree, *The Geometry of Biological Time*, Interdiscip. Appl. Math. 12, Springer, 2001.
[38] E. Zavala, K. C. Wedgwood, M. Voliotis, J. Tabak, F. Spiga, S. L. Lightman, and K. Tsaneva-Atanasova, *Mathematical modelling of endocrine systems*, Trends Endocrinology Metabolism, 30 (2019), pp. 244–257.